Modeling and Validation of Failure Behaviors of Composite Laminate Components using MAT_262 and User Defined Cohesive Model

Masato Nishi[1], Tsuyoshi Nishihara[2], Masato Iimori[1], Chikara Kawamura[2], Shunsuke Kanemoto[2], Kei Saito[1], Stefan Hartmann[3]
[1]*JSOL Corporation*
1-8-12, Harumi, Chuo-ku, Tokyo 104-6205, Japan
[2]*Mazda Motor Corporation*
3-1, Shinchi, Fuchu-cho, Aki-gun Hiroshima, 730-8670, Japan
[3]*DYNAmore Corporation*
Industriestr. 2, 70565 Stuttgart-Vaihingen, Germany

Abstract

The objective of the present study is to develop a finite element (FE) approach to predict the changes in failure behavior of a unidirectional carbon fiber reinforced plastic (CFRP) material for different laminate configurations in LS-DYNA®. Damage related parameters for an intra-lamina material model are often adjusted by reverse engineering. However, in our study, we identified these parameters in material type 262 based on a crack resistance curve, which shows the relationship between fracture toughness and crack length. A user defined cohesive zone model was also developed to take into account anisotropic inter-laminar fracture toughness depending on the fiber orientation. The changes in fracture behavior observed in the different laminate configurations in experiments can be represented in four-point bending simulations of a CFRP laminated component using the developed FE model.

Introduction

Automotive companies are interested in carbon fiber reinforced plastic (CFRP) as one of the break-through technologies that achieves a high level of downsizing, weight reduction and safety. CFRP is a light material, but has high stiffness and strength, compared to steel and aluminum. Additionally, it shows nearly ideal performance with constant load response [1-3]. Crash simulation is especially important in automotive design because of the strict regulations which specify passive safety requirements. With frontal impact, the crash energy is mainly absorbed by the deformation of axial compression. On the other hand, with side impact, bending deformation is the dominant deformation mode. So, the numerical predictions of bending fracture and axial crush deformations of a composite structure are both of great interest with increasing applications in car design.

Failure behavior of a CFRP material is the consequence of the complex damage progression of each constituent, such as fiber fracture and kinking, matrix cracking and delamination [2, 3]. These damages cause microscopic separation in the material and elasticity is lost due to a decrease in the effective area which can bring stresses. In practical use of numerical simulation, it is quite difficult to model these small scale discontinuities because of numerical issues such as the needs of complex numerical technique and computational cost, and numerical instability. One practical simulation strategy for small scale damages is modelling based on continuum damage mechanics (CDM) [4]. In this method, damage accumulation is considered in a representative unit element, which can be treated as a part of a continuum body. Therefore, CDM is familiar to finite element (FE) algorithms and easily implemented in constitutive models. Actually, many existing FE modelling of composite structures are based on CDM for intra-lamina material [5].

On the other hand, it is difficult to identify damage parameters related to stress softening after the maximum stress is applied on a physical basis. Thus, in most cases, these parameters are identified by reverse engineering, which adjusts parameters to fit the damage/failure reactions in experiments at component level. There is no established simulation technology that is able to predict the damage/failure behaviors of a CFRP structure. For example, Feraboli [6] performed an axial crushing simulation of CFRP structure using a multi-layered shell model in which shell elements were stacked and the interfaces between shell elements were connected by a cohesive zone model (CZM). However, the load response of the experiment was reproduced by adjusting the damage related parameters. Also, considering the parameters in the automotive design stage, there is a possibility that more efficient energy absorption performance can be achieved by designing not only the tube geometry and choice of material but also the laminate configuration. It has been reported that the laminate configuration affects the fracture mode and the determined mode has a great influence on the reaction force and energy absorption [2, 3]. Therefore, a numerical model which can predict the failure process and mode according to the design parameters, including changes in laminate configuration, would be valuable for designing composite products. However, Reuter [7] reported that it was necessary to adjust the damage parameters for each lamination configuration. The point is it is difficult to predict the crash performance of CFRP laminate structure by FE simulation when changing the laminate configuration at the design stage.

The objective of the present study is to develop an FE approach to predict the changes in failure behavior of a unidirectional (UD) CFRP material for different laminate configurations in LS-DYNA. We enhanced material type 262 (*MAT_262) and developed a user defined CZM. As mentioned above, damage related parameters for an intra-lamina material model are often adjusted by reverse engineering. However, in this study, we identified these parameters in *MAT_262 based on the crack resistance curve (*R*-curve). The *R*-curves for tension and compression in fiber direction were derived from double notched tensile and compression tests with different size specimens, using the size effect of fracture toughness. The user defined CZM developed here takes into account anisotropic inter-laminar fracture toughness depending on the fiber orientation. We performed four-point bending simulations of a CFRP laminated component using the developed model and verified by means of comparing with experiments. The changes in fracture behavior observed in the different laminate configurations can be represented.

FE modeling for UD laminate CFRP

For composite laminate modeling with LS-DYNA, there are three choices. The first one is a single-layered shell model with *PART_COMPOSITE, in which we can model the multi-layer laminate composite with only one-layer of shell elements, by defining information for each layer to the integration point through the thickness. It's numerically cheap and easily applied to a full vehicle model, but it is not able to describe the delamination between plies. The second one is called multi-layer shell model where each ply is modeled by shell elements and delamination is modeled by CZM. The third one is a meso/micro-scale model in which fiber and plastic are directly modeled, but huge computation cost is needed if we simulate the component model.

In the single-layered and multi-layered shell models, the intra-ply material model needs to treat the CFRP as an anisotropic homogeneous material, therefore it needs to consider anisotropic material properties, anisotropic failure law and strain softening due to damage in each direction. In LS-DYNA, some material models such as *MAT_054, 058, 261 and 262, can be applied to continuous CFRP material. For *MAT_054 and 058, generally, an approach has been applied to adjust the damage related parameters to fit the reaction in component experiments by reverse engineering. On the other hand, for *MAT_261 and 262, the approach was proposed to identify damage properties based on the experimental results to measure the fracture toughness [8, 9].

Figure 1 summarizes modelling approaches that we can select in LS-DYNA. In terms of laminate modeling that can be simulated, the reaction and failure mode for the composite component level by realistic computational costs, we selected the multi-layered shell model with *MAT_262, which was developed by Maimí [8, 9].

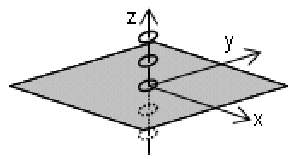

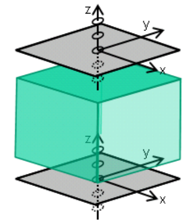

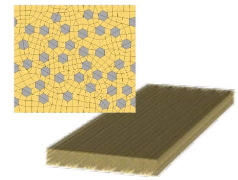

	Single-layered shell elements with *PART_COMPOSITE		Multi-layered shell elements with cohesive elements		Micro/Meso scale model
	*MAT_054/058	*MAT_261/262	*MAT_054/058	*MAT_261/262	
Lamination configuration	✓	✓	✓	✓	✓
Delamination			✓	✓	✓
Crack propagation		✓		✓	✓
Computation cost	Full vehicle level		Component level		RVE level

Figure 1: Summary of modelling approaches in LS-DYNA.

Material Characterization

The procedure for determining each parameter of the multi-layered shell model, which consists of intra-lamina and inter-lamina models of Toray 3252S-10 (T700/2592) is described in this section.
Table 1 summarizes the material parameters required for *MAT_262, identified values and material experiments performed to identify these parameters. Parameters related to stress-strain characteristics, E_A, E_B, PR_{BA}, G_{AB}, SIG_Y, E_{TAN}, and maximum stress, X_T, Y_T, S_L, X_C, Y_C in each direction were determined from tensile and compressive coupon tests in 0, +/-45 and 90 degree directions (JIS K7164, JIS K7076). The tensile and compressive fracture toughness in matrix direction, G_{YT}, G_{YC}, and shear fracture toughness, G_{SL}, were determined from four-point end notched flexure (4-ENF) [10] and double cantilever beam (DCB). The tensile damage parameters, G_{XT}, X_{TO}, G_{XTO}, and compressive damage parameters, G_{XC}, X_{CO}, G_{XCO}, in the fiber direction are identified based on the *R*-curve, which shows the relationship between fracture toughness and crack length. In this study, instead of commonly used compact tension (CT) and compact compression (CC), we characterized *R*-curve using the size effect of fracture toughness by double notched specimens with different sizes by Catalanotti [11, 12]. Then, according to the procedure proposed by Dávila [13], we approximate the *R*-curve characterized from the experiments to the trilinear curve using the following equations and determined the damage parameters.

$$G_M(\Delta a) = \begin{cases} \frac{3}{2}\frac{\Delta a}{l_c}G_c & if \ \frac{\Delta a}{l_c} \leq \frac{3}{2}\frac{m}{n} \\ mG_c + (1-n)\frac{3}{2}\frac{\Delta a}{l_c}G_c & if \ \frac{3}{2}\frac{m}{n} < \frac{\Delta a}{l_c} < \frac{3}{2}\frac{1-m}{1-n} \\ G_c & if \ \frac{\Delta a}{l_c} \geq \frac{3}{2}\frac{1-m}{1-n} \end{cases} \quad (1)$$

Here, $l_c=\gamma E G_c/\sigma_c^2$, where σ_c and G_c are the strength and the fracture toughness in the steady state, respectively. γ, m, n are dimensionless parameters for trilinear approximation.

Figure 2 shows the compressive and tensile Toray 3252S-10 specimens prior to testing. A total of 108 samples were used composed of 72 compressive and 36 tensile specimens. An extended experimental campaign was conducted to measure the fracture toughness under compression with a total of 72 specimens due to the high scatter observed in the measured data. Figure 3 shows the results of applying this methodology to obtain the compressive and tensile *R*-curves calculated using the average maximum load of the test results. In compression, the value of the fracture process zone is 16.88 mm and the measured fracture toughness is 97.44 N/mm. In tension, the value of the fracture process zone is 2.22 mm and the measured fracture toughness is 182.13 N/mm. Trilinear approximations for identification of damage related parameters are also shown in Figure 3. The approximate parameters in Equation (1) are m = 0.275, n = 0.788, γ = 0.65 for compression, and m = 0.35, n = 0.72, γ = 0.40 for tension.

Table 1: MAT262 input parameters for material properties.

Variable	Definition	T700/2592	Experiment
E_A	Young's modulus in longitudinal direction	129 GPa	From tensile coupon test in 0° direction
X_T	Longitudinal tensile strength	3036 MPa	
E_B	Young's modulus in transverse direction	8.9 GPa	Tensile coupon test in 90° direction
PR_{BA}	Poisson's ratio, ν_{21}	0.023	
Y_T	Transverse tensile strength	47.9 MPa	
G_{AB}	In-plane shear modulus, G_{12}	4.6 GPa	Tensile coupon test in 45° direction
SIG_Y	In-plane shear yield stress	52 MPa	
E_{TAN}	Tangent modulus for in-plane shear plasticity	230 MPa	
S_L	In-plane shear strength	100 MPa	
X_C	Longitudinal compressive strength	1301 MPa	Compressive coupon test in 0°
Y_C	Transverse compressive strength	148 MPa	Compressive coupon test in 90°
PR_{CA}	Poisson's ratio, ν_{31}	0.023	Assumed equal to PR_{BA}
PR_{CB}	Poisson's ratio, ν_{32}	0.4	Assumed 0.4
G_{BC}	Out-of-plane shear modulus, G_{23}	3.2 GPa	Calculated using E_A, E_B and PR_{BA}
G_{CA}	Out-of-plane shear modulus, G_{31}	4.6 GPa	Assumed equal to G_{AB}
G_{XT}	Fracture toughness for longitudinal tension	131 N/mm	Testing methodology described in [12] , and identified according to [13]
X_{TO}	Longitudinal tensile strength at inflection point	353 MPa	
G_{XTO}	Fracture toughness for longitudinal tension to define bi-linear damage	52 N/mm	
G_{XC}	Fracture toughness for longitudinal compression	66 N/mm	Testing methodology described in [11], and identified according to [13]
X_{CO}	Longitudinal compressive strength at inflection point	181 MPa	
G_{XCO}	Fracture toughness for longitudinal compression to define bi-linear damage	32 N/mm	
G_{YT}	Fracture toughness for transverse tension	0.28 N/mm	DCB test in 0°
G_{SL}	Fracture toughness for in-plane shear	1.4 N/mm	4-ENF [10] in 0°
G_{YC}	Fracture toughness for transverse compression	2.3 N/mm	Calculated using G_{SL} according to [8]

For delamination, we applied the CZM of the mixed mode bilinear type tension-separation law implemented in LS-DYNA as *MAT_138. Here, we defined Mode I strength as the same value as tensile strength in 90 degrees, and Mode I fracture toughness is characterized from the result of a double cantilever beam test. Furthermore, we conducted a simulation under the same conditions as the DCB test and confirmed that the simulated response was the same as the experimental response for these inputted parameters. For Mode II, fracture toughness is determined from 4-ENF test. Again, we confirmed the validity of the determined parameters by conducting 4-ENF simulation.

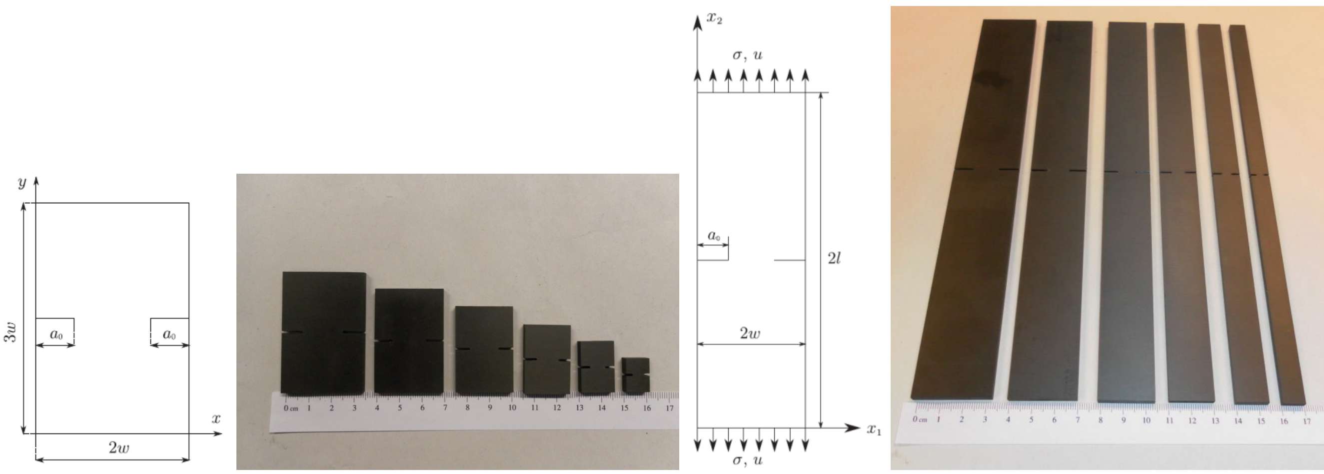

Figure 2: One sample of each set of double notched specimens, compression (left), tension (right).

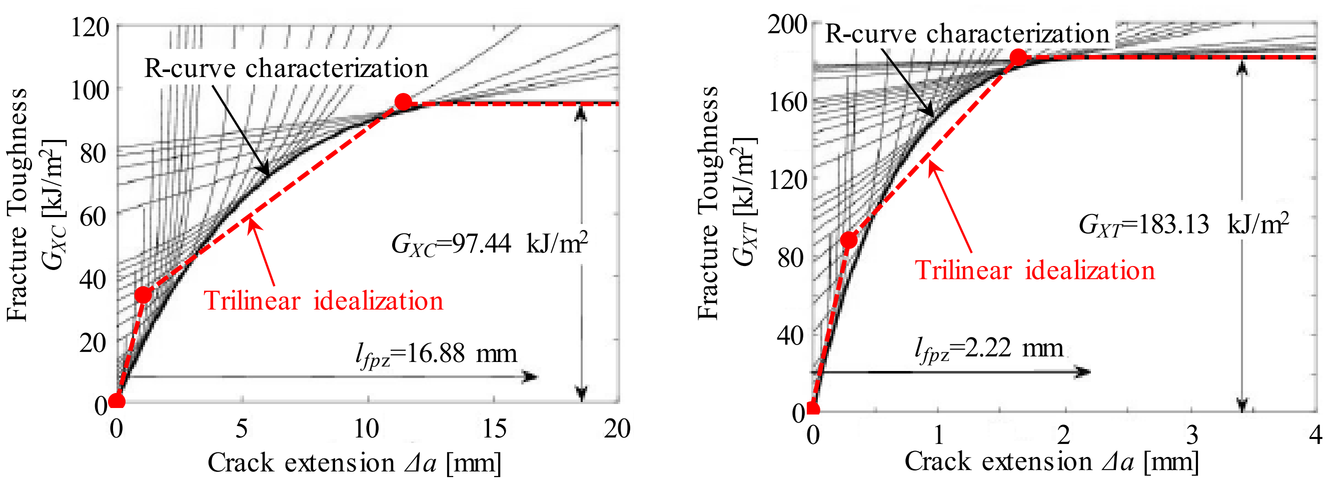

Figure 3: Relationship between fracture toughness and crack extension for Toray 3252S-1, using size-effect low compression (left), tension (right).

1st Experimental Validation

After constructing a material model for each ply and characterizing the inter-laminar delamination between plies, we conducted the bending simulation of a CFRP laminate beam in LS-DYNA and compared it to the experiment results. The four-point bending test was performed quasi-statically (20 mm/min.) using a universal testing machine, SHIMADZU UH200XR, as shown in Figure 4. Specimens with two types of laminated configuration were prepared to observe the failure modes in the different laminate configurations. One is a quasi-isotropic $[0/45/90/-45]_{3S}$ laminate, the other is mainly 0 degree $[0/90/90/(0)_9]_S$. Both laminate beam specimens were made of a total 24 layers and reinforcing tabs $[0/45/90/-45]_{2S}$ were added to the ends of the specimen beam as shown in Figure 5 (left). The cross section of the half cylindrical shape is as shown in Figure 5 (right). Figure 6 shows the experimental failure modes with the quasi-isotropic and 0 main laminates. In the quasi-isotropic laminate specimen, the fracture occurred on the surface at the edge of the depression, and it propagates in the circumferential direction and under the impactor. On the other hand, in the 0 main laminate specimen, cracks propagated in the longitudinal direction and a significant decrease in load was observed. We observed obviously different failure modes depending on the two different laminate configurations.

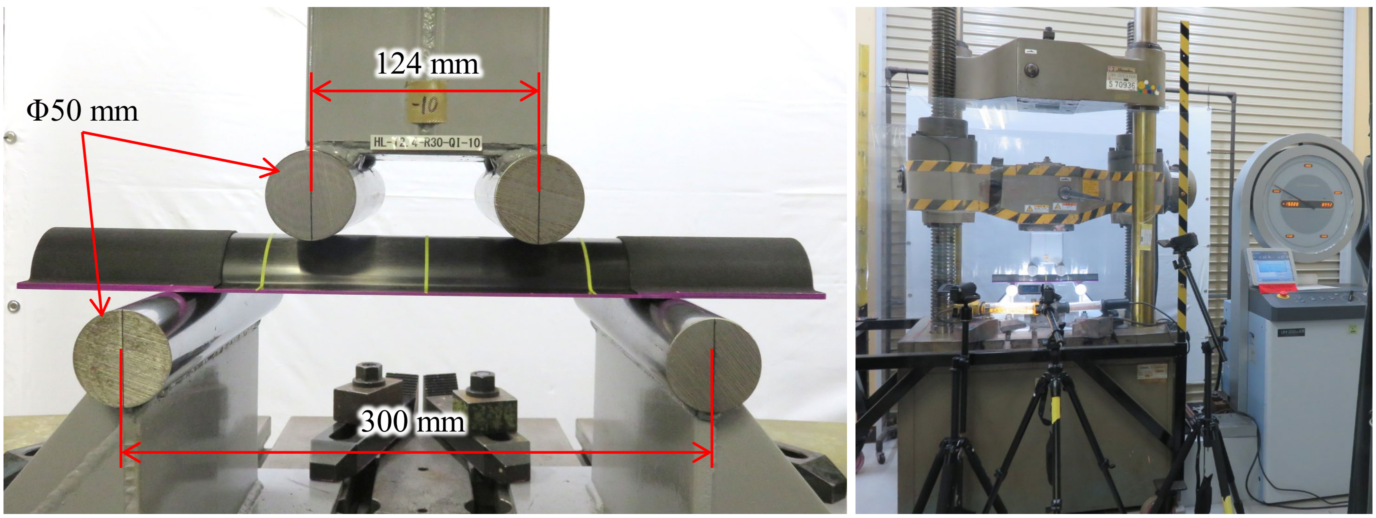

Figure 4: Test setup of four-point bending of UD laminate beam.

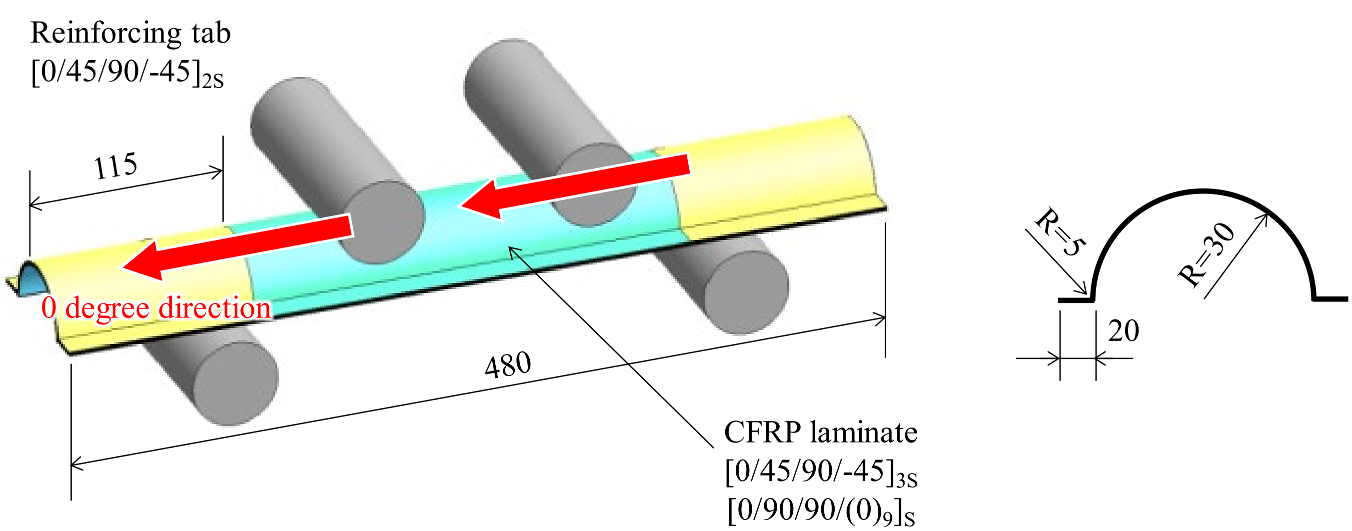

Figure 5: Dimension of UD laminate beam, four-point bending model (left), cross section (right).

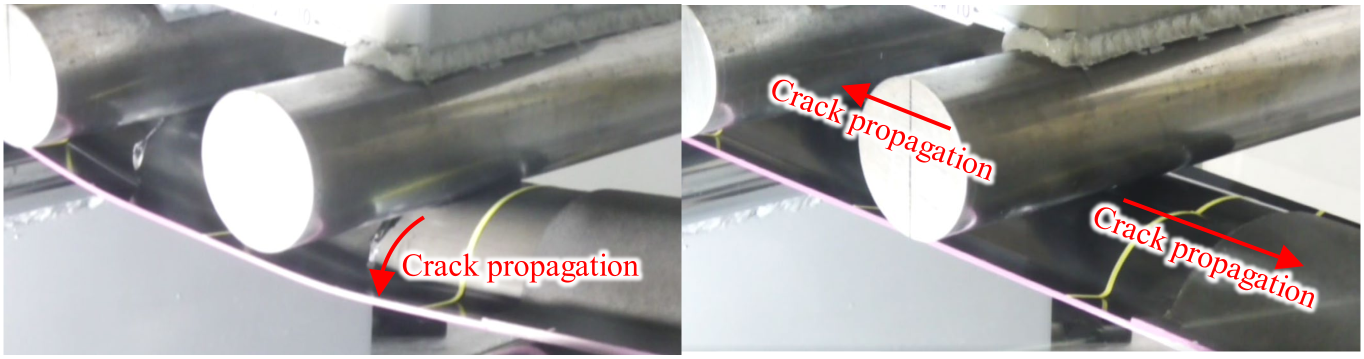

Figure 6: Experimental failure modes, quasi-isotropic [0/45/90/-45]$_{3S}$ (left), 0 main [0/90/90/(0)$_9$]$_S$ (right).

In the multi-layered shell model, each of the 24 layers is modeled by shell elements and delamination in between each shell layer is modeled by CZM. The mesh size is about 1 mm, and the total number of shell and cohesive elements is about 4 million. The calculation time was about 26 hours by 128 cores with MPP LS-DYNA calculation.

Figure 7 shows a comparison of the force–displacement curves between experiment and simulation (left) and simulated failure behaviors with the quasi-isotropic laminate (right). We can see quite good agreement with the load response obtained in the experiment, where the load gradually decreases after the maximum load is shown at the stroke of around 10 mm. The experimental photo in Figure 6 (left) is the appearance of the specimen, whereas the simulation results show the damage value. We can confirm that the simulated initiation point and the crack propagation path are in good agreement with the bending experiment.

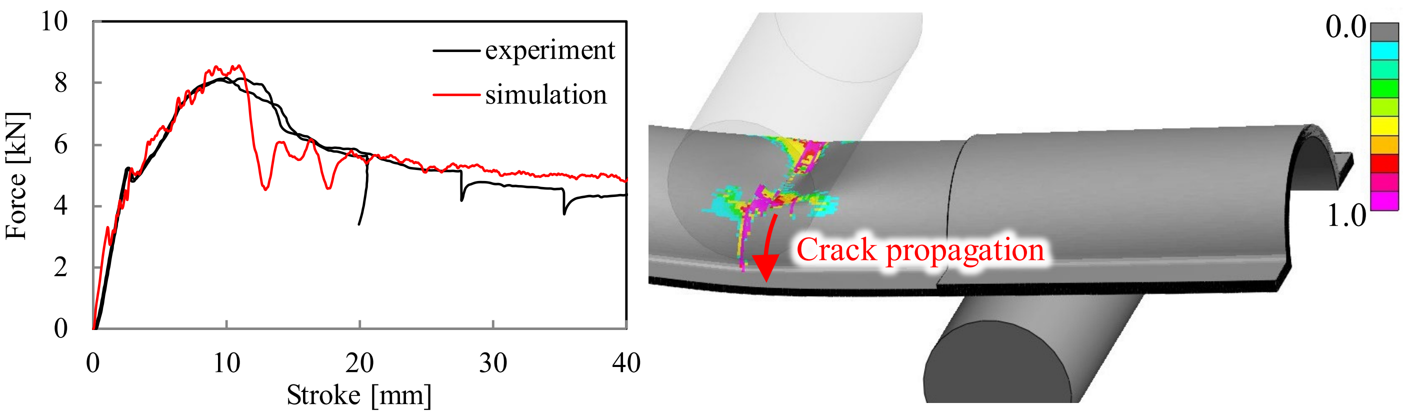

Figure 7: Simulation result with [0/45/90/-45]$_{3S}$, force-displacement curve (left), failure deformation (right).

Figure 8 shows a comparison of the force–displacement curves and simulated failure behaviors with the 0 main laminate. Simulated failure mode and load response are not able to capture the experimental response. In the simulation, we can see the depression under impactor and fracture progresses in the circumferential direction, as observed in quasi-isotropic laminate. Also, the rapid load drop due to the crack propagation in the longitudinal direction in the experiment is not simulated.

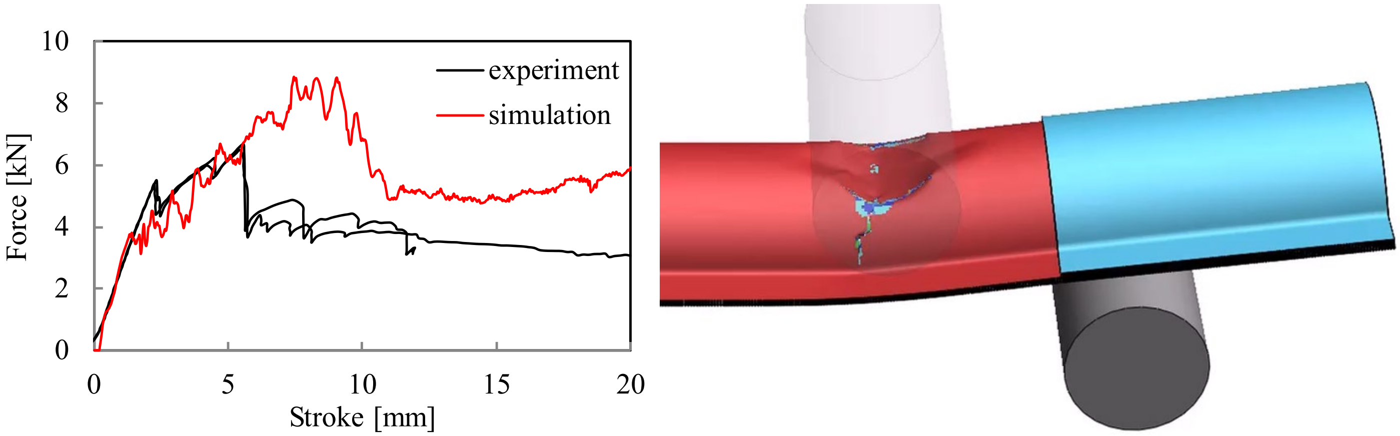

Figure 8: Simulation result with $[0/90/90/(0)_9]_S$, force-displacement curve (left), failure deformation (right).

Review and Improvement of FE Modeling

First, in order to correctly understand the different failure modes between the quasi-isotropic and 0 main laminate specimens, after the experiments, the specimens were photographed with X-ray CT, SHIMADZU inspeXio SMX-225CT FPD HR. Figure 9 (left) shows the internal failure of a quasi-isotropic specimen at the cross section just below the impactor, and Figure 9 (right) shows one of the 0 main specimens at the same cross section. We understood that, in the quasi-isotropic specimen, inter-laminar failures occur everywhere through the laminate thickness. On the other hand, in the 0 main specimen, a sharp transverse crack within the 0 degree layers and delamination only occurring between the lower 0//90 layers were observed. To represent the transverse shear crack observed within 0 degree layers, we added transverse damage for 23-plane and 31-plane into *MAT_262 as an optional card.

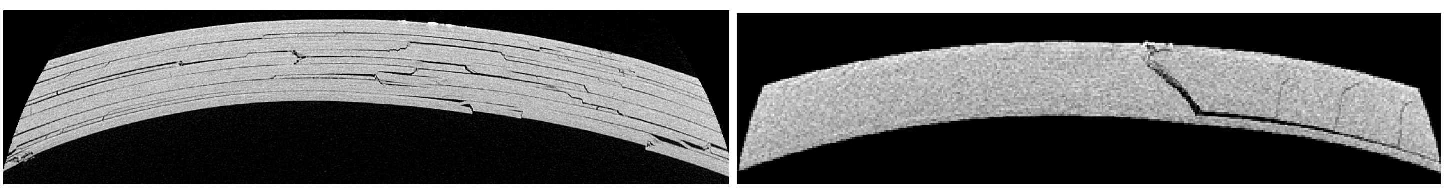

Figure 9: Internal failures observed with X-CT measurement, $[0/45/90/-45]_{3S}$ (left), $[0/90/90/(0)_9]_S$ (right).

The next point is delamination modelling. In the first simulation of the 0 main laminate, we confirmed that there were a lot of delaminations, but no transverse crack in thickness direction. However, in the experiment, as shown in Figure 9 (right), delamination only occurred between the lower 0//90 interface.

Some literatures [14] reported that the fracture toughness is larger when delamination propagates in the 90//90 direction than when propagating in the 0//0 direction. However, in our first experimental validation, we used an isotropic CZM in which delamination propagates with the same energy release ratio in every direction. Additionally, the fracture toughness defined in the CZM was identified by DCB and 4-ENF testes where the delamination propagated between layers in the 0//0 direction. Therefore, we considered that delamination within 0 degree layers in the 90//90 direction easily developed.

To overcome this problem, we developed a user defined CZM that takes into account anisotropic inter-laminar fracture toughness depending on the crack propagation angle for fiber orientation. Figure 10 shows the flow chart of the developed CZM. This model is the same bilinear mixed mode CZM as *MAT_138, but we applied an algorithm to distinguish the delamination propagated directions of Mode I and II and change the fracture toughness depending on the propagation direction. Here, Mode I opening direction is calculated from four in-plane integration points. Mode II direction is calculated from shear deformations within each integration point.

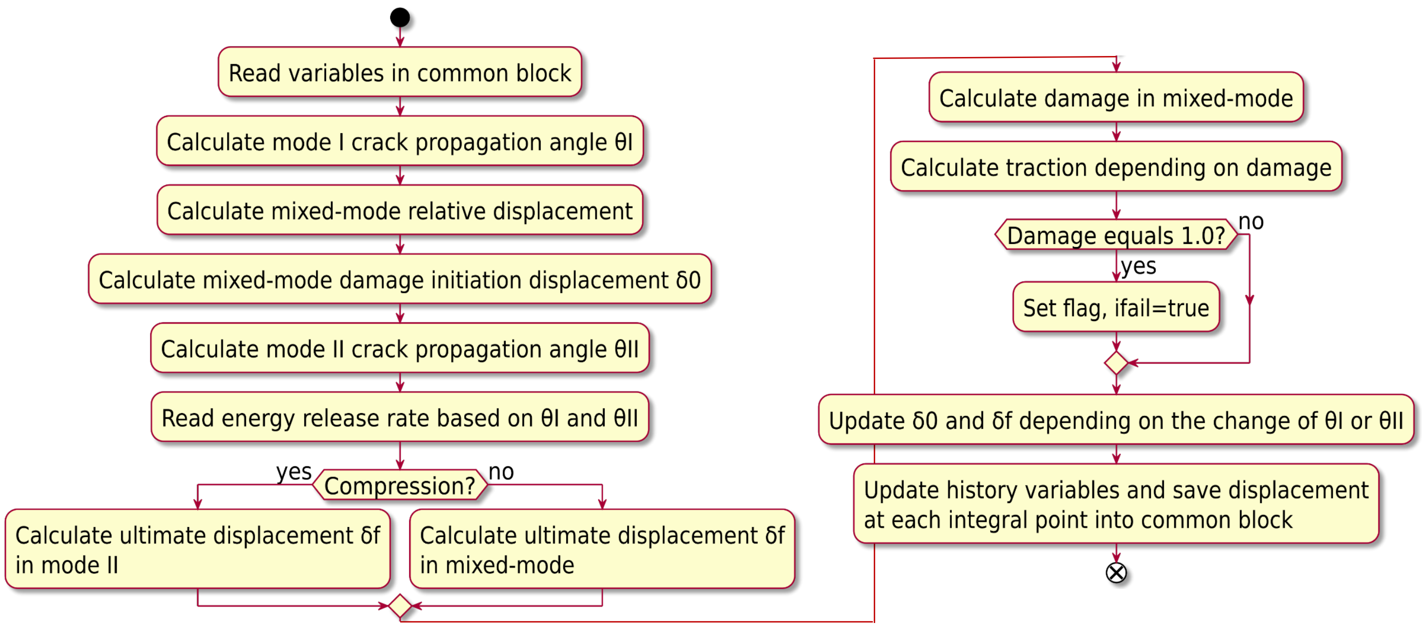

Figure 10: Flowchart of user defined anisotropic CZM.

Finally, we reviewed the validity of laminate modeling. The reason for reviewing the laminate model is that our first model could not show the deformation mode in which the cross section opens. But we considered this open mode to be an important deformation to reproduce the crack propagation in the longitudinal direction. In our first multi-layered shell model, cohesive elements have a thickness because cohesive elements were simply modeled with nodes consistent with the shell elements. As a result, as shown in Figure 11, the shape of the cohesive elements was rectangular in the longitudinal direction, but in the half-cylinder cross section, the thick cohesive elements had to be modeled as an inclined element.

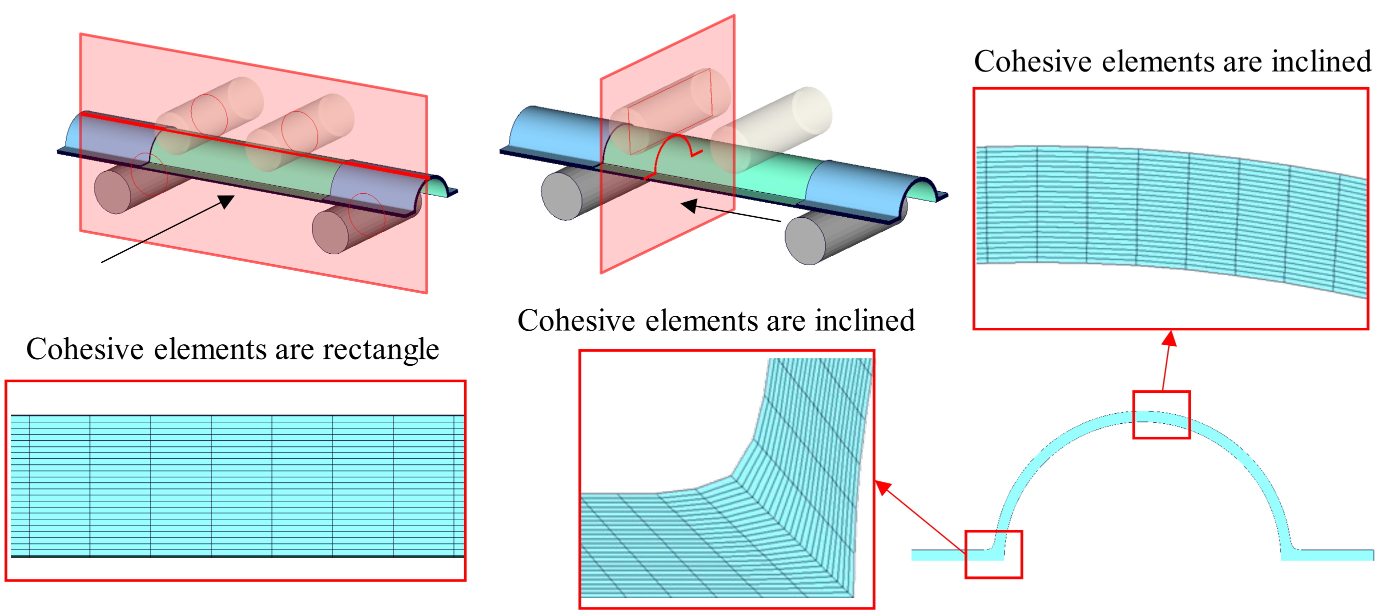

Figure 11: Laminate modeling for 1st experimental validation, cohesive elements in longitudinal direction (left), cohesive elements in half-cylinder cross section (right).

To verify that the bending stiffness of the multi-layered shell model connected with the inclined cohesive element, a simple numerical study was performed as shown in Figure 12. The first model is a layered shell connected by a rectangular cohesive element. The second is a model in which the nodes of the upper and lower shell elements are shifted, and the cohesive elements between the layers are inclined. The third model is a model in which the nodes of the upper and lower shell elements are shifted, but the layers are connected by tied-offset contacts. The fourth model is a model in which the shell elements' upper and lower nodes are also shifted, and these are connected to a tied-offset contact and a zero-thick cohesive element.

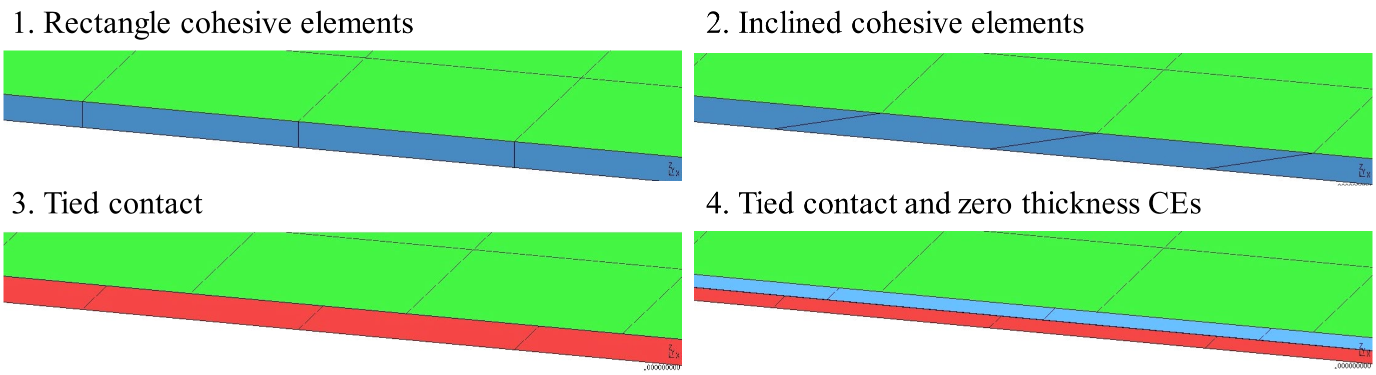

Figure 12: numerical verification for multi-layered shell model.

We could confirm that the stress distribution of the cantilever model became abnormal only when the layered shells are connected with inclined cohesive elements. Actually, we wanted to use the tied offset and zero-thickness cohesive element modeling in the component simulation. But we applied tentatively thick shells and zero thickness shells in the second validation, since the numerical instability could not be overcome in the component model with tied contact and zero thickness cohesive elements.

2nd Experimental Validation

For our second experimental validation, we used the improved FE model in which the transverse shear damage in *MAT_262 and the developed anisotropic user defined CZM are used. And, since the numerical instability could not be overcome, tentatively thick shells and zero thickness shells were used. The calculation time was about 82 hours by 128 cores with MPP LS-DYNA calculation.
Figure 12 (left) shows a comparison of the force-displacement curve between experiment, the first simulation and the second simulation by applying the three modifications. The improved FE model can capture the load response observed in experiments. Figure 12 (right) shows a simulated failure mode where the longitudinal crack propagation observed in the experiment is also represented.

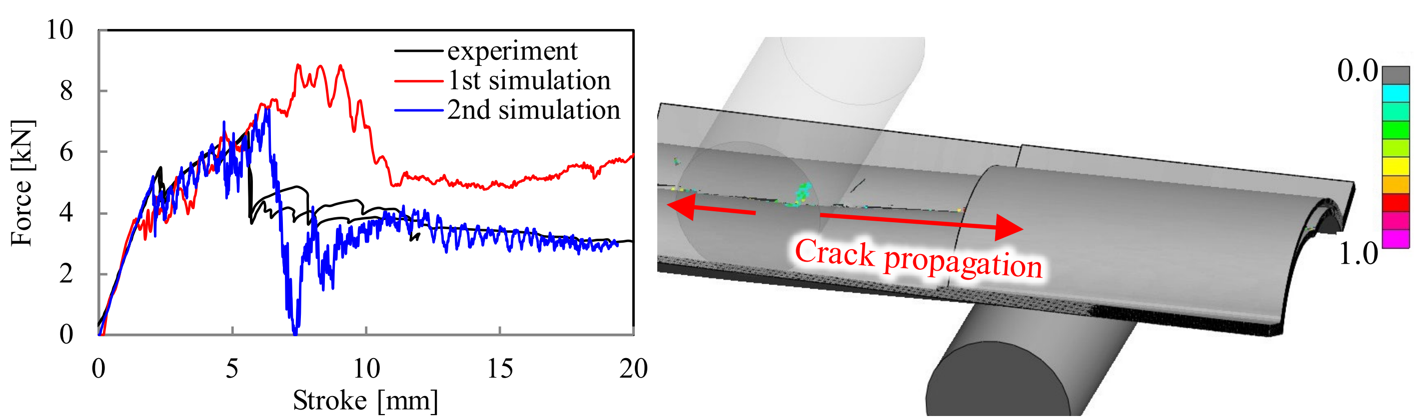

Figure 12: Simulation results by applying the three modifications.

Summary & Future Work

In this study, we have confirmed that different failure modes occur depending on the lamination configuration of UD laminate beams. And by adding three improvements, enhancement of material model, development of anisotropic CZM and modification for laminate model, finally, we could represent the change in the failure mode due to the laminated configuration with the improved FE model.
For future works, the characterization of direction-dependent inter-lamina fracture toughness is still ongoing. And we have to improve the numerical instability with tied contact and zero-thickness cohesive elements because the computation cost with thick shells is very large and it is not acceptable to apply to vehicle crash simulation. Additionally, we already conducted experiments for different cross sections and laminate configurations, and plan to validate this model to those experimental results.

References

[1] A. Elmarakbi, Advanced Composite Materials for Automotive Applications: Structural Integrity and Crashworthiness, John Wiley & Sons, Ltd (2013).
[2] D. Hull, A unified approach to progressive crushing of fibre-reinforced composite tubes, Composites science and technology, **40**, 4, pp. 377-421 (1991).
[3] H. Hamada, S. Ramakrishna, and H. Satoh, Crushing mechanism of carbon fibre/PEEK composite tubes, Composites, **26**, 11, pp. 749-755 (1995).
[4] J. Lemaitre and R. Desmorat, Engineering damage mechanics: ductile, creep, fatigue and brittle failures, Springer Science & Business Media (2005).
[5] P. Ladeveze and E. LeDantec, Damage modelling of the elementary ply for laminated composites, Composites science and technology, **43**, 3, pp. 257-267 (1992).
[6] P. Feraboli, B. Wade, F. Deleo, M. Rassaian, M. Higgins and A. Byar, LS-DYNA MAT54 modeling of the axial crushing of a composite tape sinusoidal specimen, Composites Part A: Applied Science and Manufacturing, **42**, 11, pp. 1809-1825 (2011).
[7] C. Reuter, K. Sauerland and T. Tröster, Experimental and numerical crushing analysis of circular CFRP tubes under axial impact loading, Composite Structures, **174**, 15, pp.33–44 (2017).
[8] P. Maimí, P.P. Camanho, J.A. Mayugo and C.G. Dávila, A continuum damage model for composite laminates: Part I – Constitutive model, Mechanics of Materials, **39**, 10, pp. 897-908 (2007).
[9] P. Maimí, P.P. Camanho, J.A. Mayugo and C.G. Dávila, A continuum damage model for composite laminates: Part II – Computational implementation and validation, Mechanics of Materials, **39**, 10, pp. 909-919 (2007).
[10] R.H. Martin and B.D. Davidson, Mode II fracture toughness evaluation using four point bend, end notched flexure test, Plastics, Rubber and Composites, **28**, 8, pp. 401–406 (1999).
[11] G. Catalanotti, J. Xavier and P.P. Camanho, Measurement of the compressive crack resistance curve of composites using the size effect law, Composites Part A: Applied Science and Manufacturing, **56**, pp. 300–307 (2014).
[12] G. Catalanotti, A. Arteiro, M. Hayati and P.P. Camanho, Determination of the mode I crack resistance curve of polymer composites using the size-effect law, Engineering Fracture Mechanics, **118**, pp. 49–65 (2014).
[13] C.G. Dávila, C.A. Rose and P.P. Camanho, A procedure for superposing linear cohesive laws to represent multiple damage mechanisms in the fracture of composites, International Journal of Fracture, **158**, pp. 211–223 (2009)
[14] L. Zhao, Y. Wang, J. Zhang, Y. Gong, Z. Lu, N. Hu and J. Xu, An interface-dependent model of plateau fracture toughness in multidirectional CFRP laminates under mode I loading, Composites Part B: Engineering, **131**, 15, pp. 196-208 (2017).